THE ASTROPHYSICAL JOURNAL, 533:L57–L60, 2000 April 10

INFRARED SPECTROSCOPY OF A MASSIVE OBSCURED STAR CLUSTER IN THE ANTENNAE GALAXIES (NGC 4038/9) WITH NIRSPEC[1]

ANDREA M. GILBERT,[2] JAMES R. GRAHAM,[2] IAN S. MCLEAN,[3] E. E. BECKLIN,[3] DONALD F. FIGER,[4] JAMES E. LARKIN,[3] N. A. LEVENSON,[5] HARRY I. TEPLITZ,[6,7] AND MAVOURNEEN K. WILCOX[3]

Received 1999 October 27; accepted 2000 February 24; published 2000 March 20

ABSTRACT

We present infrared spectroscopy of the Antennae galaxies (NGC 4038/9) with the near-infrared spectrometer (NIRSPEC) at the W. M. Keck Observatory. We imaged the star clusters in the vicinity of the southern nucleus (NGC 4039) with 0.″39 seeing in the *K* band using NIRSPEC's slit-viewing camera. The brightest star cluster revealed in the near-IR [$M_K(0) \simeq -17.9$] is insignificant optically but is coincident with the highest surface brightness peak in the mid-IR (12–18 μm) *Infrared Space Observatory* image presented by Mirabel et al. We obtained high signal-to-noise ratio 2.03–2.45 μm spectra of the nucleus and the obscured star cluster at $R \sim 1900$. The cluster is very young (~4 Myr), massive ($M \sim 16 \times 10^6\ M_\odot$), and compact (with a density of ~115 $M_\odot$ pc^{-3} within a 32 pc half-light radius), assuming a Salpeter initial mass function (0.1–100 $M_\odot$). Its hot stars have a radiation field characterized by $T_{\rm eff} \sim 39{,}000$ K, and they ionize a compact H II region with $n_e \sim 10^4$ cm^{-3}. The stars are deeply embedded in gas and dust ($A_V \sim 9$–10 mag), and their strong far-ultraviolet field powers a clumpy photodissociation region with densities $n_{\rm H} \gtrsim 10^5$ cm^{-3} on scales of ~200 pc, radiating $L_{\rm H_2\ 1-0\ S(1)} = 9600\ L_\odot$.

Subject headings: galaxies: individual (NGC 4038/9) — galaxies: ISM — galaxies: starburst — galaxies: star clusters — H II regions — infrared: galaxies

1. INTRODUCTION

The Antennae (NGC 4038/9) are a pair of disk galaxies in an early stage of merging that contain numerous massive super–star clusters (SSCs) along their spiral arms and around their interaction region (Whitmore & Schweizer 1995; Whitmore et al. 1999). The molecular gas distribution peaks at both nuclei and in the overlap region (Stanford et al. 1990), but the gas is not yet undergoing a global starburst that is typical of more advanced mergers (Nikola et al. 1998). Star formation in starbursts appears to occur preferentially in SSCs. We chose to observe the Antennae because their proximity permits an unusually detailed view of the first generation of merger-induced SSCs and their influence on the surrounding interstellar medium (ISM).

The *Infrared Space Observatory* (*ISO*) 12–18 μm image shows that the hot dust distribution is similar to that of the gas but peaks at an otherwise inconspicuous point on the southern edge of the overlap region (Mirabel et al. 1998). This powerful starburst knot is also a flat-spectrum radio continuum source (Hummel & van der Hulst 1986) and may be associated with an X-ray source (Fabbiano, Schweizer, & Mackie 1997). We imaged the region around this knot and discovered a bright compact star cluster coincident with the mid-IR peak. We obtained moderate-resolution ($R \sim 1900$) *K*-band spectra of both the obscured cluster and the NGC 4039 nucleus.

2. OBSERVATIONS AND DATA REDUCTION

The new facility near-infrared spectrometer (NIRSPEC; 0.95–5.6 μm) on the Keck II telescope was commissioned during 1999 April–July by McLean et al. (1998). It has a cross-dispersed cryogenic echelle with $R \sim 25{,}000$ and a low-resolution mode with $R \sim 2000$. The spectrometer detector is a 1024 × 1024 InSb ALADDIN focal-plane array, and the IR slit-viewing camera detector is a 256 × 256 HgCdTe PICNIC array.

We observed the Antennae with NIRSPEC during the 1999 June commissioning run. Slit-viewing camera (SCAM) images at 2 μm reveal that the mid-IR *ISO* peak is a bright (K = 14.6) compact star cluster located 20.″4 east and 4.″7 north of the *K*-band nucleus. This cluster is associated with a faint (V = 23.5) red ($V-I$ = 2.9) source (number 80 in Whitmore & Schweizer 1995) visible with the Space Telescope (B. C. Whitmore & Q. Zhang 1999, private communication). We obtained low-resolution ($R \simeq 1900$) $\lambda \simeq 2.03$–2.45 μm spectra through a 0.″57 × 42″ slit at a position angle of 77° located on the obscured star cluster and the nucleus of NGC 4039. The total integration time on source was 2100 s.

We dark-subtracted, mean sky-subtracted, flat-fielded, and corrected two-dimensional spectra for bad pixels and cosmic rays before rectifying the curved order onto a grid in which wavelength and slit position are perpendicular. We then corrected for residual sky emission and divided by a B1.5 standard star spectrum to correct for atmospheric absorption. The object spectra were extracted using a Gaussian weighting function matched to their wavelength-integrated profiles (intrinsic

[1] Data presented herein were obtained at the W. M. Keck Observatory, which is operated as a scientific partnership among the California Institute of Technology, the University of California, and the National Aeronautics and Space Administration. The Observatory was made possible by the generous financial support of the W. M. Keck Foundation.

[2] Department of Astronomy, 601 Campbell Hall, University of California, Berkeley, Berkeley, CA 94720-3411; agilbert@astro.berkeley.edu.

[3] Department of Physics and Astronomy, UCLA, Los Angeles, CA 90095-1562.

[4] Space Telescope Science Institute, 3700 San Martin Drive, Baltimore, MD 21218.

[5] Department of Physics and Astronomy, Johns Hopkins University, Baltimore, MD 21218.

[6] Laboratory for Astronomy and Solar Physics, Code 681, Goddard Space Flight Center, Greenbelt, MD 20771.

[7] NOAO Research Associate.

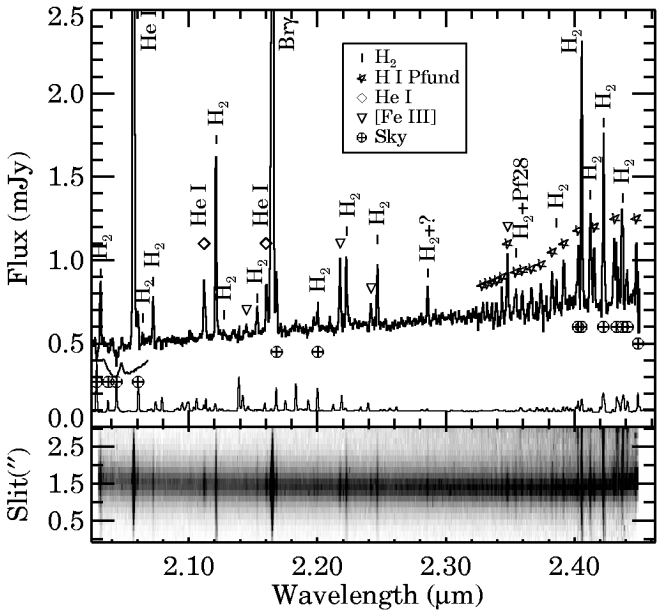

FIG. 1.—NIRSPEC spectrum of the obscured star cluster showing nebular and fluorescent H_2 emission with a continuum rising toward the red. The scaled sky counts are plotted at 0.1 mJy. The ω-shaped curve represents an atmospheric CO_2 band at 2.05 μm.

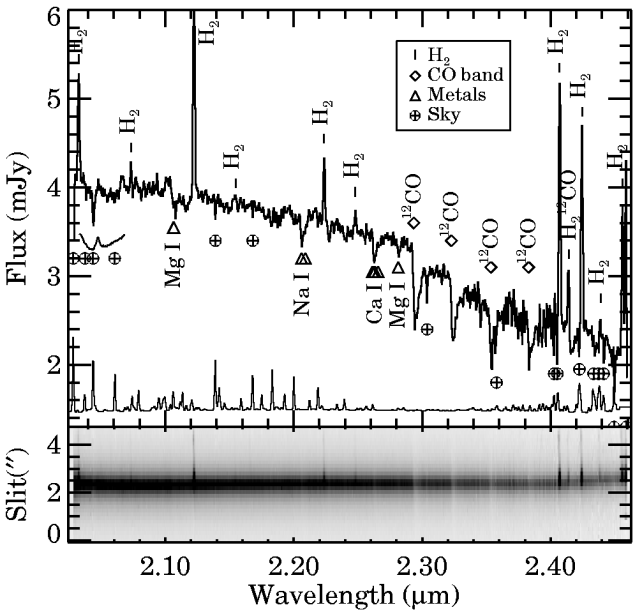

FIG. 2.—NIRSPEC spectrum of NGC 4039 nucleus showing extended collisionally excited H_2 emission and a strong stellar continuum marked by photospheric absorption. No Brγ is present. The scaled sky counts are shown at 1.5 mJy.

FWHM = 0.″84 for the cluster and 0.″99 for the nucleus),[8] and then an aperture correction was applied to recover the full flux in the continua. Thus, we neglected the more extended H_2 emission, which has a maximum FWHM $\sim$ 1.″7 in the cluster and $\sim$1.″2 in the nucleus. We obtained a flux scale by requiring the 2.2 μm star flux to equal that corresponding to its K magnitude. Reduced spectra are shown in Figures 1 and 2.

3. MASSIVE STAR CLUSTER

The cluster spectrum is characterized by strong emission lines[9] and a continuum (detected with a signal-to-noise ratio [S/N] $\simeq$15) that is dominated by the light of hot blue stars and dust. The nebular emission lines are slightly more extended than the continuum, and the H_2 emission is even more extended. This suggests a picture in which hot stars and dust are embedded in a giant compact H II region surrounded by clumpy (see § 3.2) clouds of obscuring gas and dust whose surfaces are ionized and photodissociated by far-ultraviolet (FUV) photons escaping from the star cluster.

For a distance to the Antennae of 19 Mpc (H_0 = 75 km s^{-1} Mpc^{-1} and 1″ = 93 pc; Whitmore et al. 1999), we find that the cluster has $M_K = -16.8$. We estimate the screen extinction to the cluster by assuming a range of $(V-K)_0 \simeq 0$–1, as expected from Starburst99 models (Leitherer et al. 1999), and that $A_K = 0.11A_V$ (Rieke & Lebofsky 1985). We find that A_V = 9–10 mag, which implies $M_K(0) = -17.9$, adopting A_K = 1.1 (which is confirmed by our analysis of the H II recombination lines in § 3.1). We can use the intrinsic brightness along with the Lyman continuum flux inferred from the dereddened Brγ flux (3.1×10^{-14} ergs s^{-1} cm^{-2}), $Q(H^+)_0$ = 1.0×10^{53} photons s^{-1}, to constrain the cluster mass and age. Using instantaneous Starburst99 models, we find a total mass of $\sim 7 \times 10^6$ $M_\odot$ (with $\sim$2600 O stars) for a Salpeter initial mass function extending from 1 to 100 $M_\odot$ and an age of $\sim$4 Myr. This age is consistent with the lack of photospheric CO and metal absorption lines from red supergiants and other cool giants, which would begin to contribute significantly to the 2 μm light at an age of $\sim$7 Myr (Leitherer et al. 1999). The cluster's density is then about 115 $M_\odot$ pc^{-3} for stars of 0.1–100 $M_\odot$ within a half-light radius of 32 pc. This density is 30 times less than that of the LMC SSC R136 (within a radius of 1.7 pc, assuming a Salpeter proportion of low-mass stars; Hunter et al. 1995). Thus, the Antennae cluster may be a complex of clusters rather than one massive cluster.

3.1. *Nebular Emission*

The cluster spectrum features a variety of nebular lines that reveal information about the conditions in the ionized gas around the cluster, which in turn allows us to constrain the effective temperature of the ionizing stars. The lack of a strong Pfund discontinuity at 2.28 μm indicates that the nebular free-free and bound-free continuum is diluted by starlight and dust emission (signaled by the rising continuum toward longer λ) in the cluster.

We detected H I Pfund series lines from Pf19 to Pf38 and display their fluxes relative to that of Brγ in Figure 3. The filled diamonds represent fluxes for the blends Pf28 + H_2 2–1 $S(0)$ and Pf29 + [Fe III]. They fall well above the other points, which follow closely the theoretical expectation for intensities relative to Brγ (*solid curve*) with no reddening applied, for a gas with $n_e = 10^4$ cm^{-3} and $T_e = 10^4$ K (Hummer & Storey 1987). Excluding the two known blends, the best-fit foreground screen extinction is $A_K = 1.1 \pm 0.3$ mag (*dashed curve*), assuming the extinction law of Landini et al. (1984) and evaluated at 2.2 μm. We consider this an upper limit on A_K because a close look at the spectrum shows that the points above

[8] These widths are greater than those measured from the SCAM images, $\sim$0.″69 and $\sim$0.″83 (intrinsic), because of the extended line contribution and rectification errors of order $\lesssim$1 pixel at the chip edges.

[9] A table of measured line fluxes is available electronically at http://astro.berkeley.edu/~agilbert.

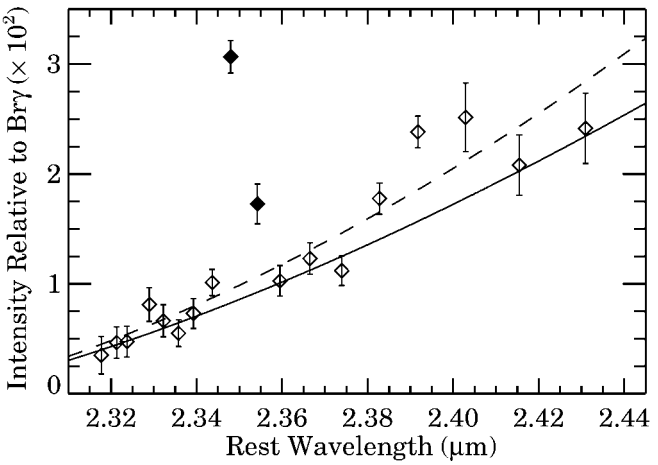

FIG. 3.—Pfund line fluxes relative to Brγ flux (1.05×10^{-14} erg s^{-1} cm^{-2}). The solid curve is the unextincted theoretical curve for $n_e = 10^4$ cm^{-3} and $T_e = 10^4$ K (Hummer & Storey 1987). The filled diamonds represent lines that are known blends, and the dashed curve shows theoretical fluxes with a best-fit extinction $A_K = 1.1$ mag.

the dashed line in Figure 3 for Pf22–24 at 2.404, 2.393, and 2.383 μm may also be blended or contaminated by sky emission, implying a lower A_K and a much better fit to the theory. Hence, the majority of the extinction toward the cluster is bypassed by observing it in the *K* band.

The ratios of [Fe III] lines are nebular density diagnostics; in Table 1, we list the observed ratios and theoretical predictions of Keenan et al. (1992) for emission from a collisionally excited 10^4 K gas, as tabulated by Luhman, Engelbracht, & Luhman (1998). The ratios of [Fe III] 2.146 μm and [Fe III] 2.243 μm to [Fe III] 2.218 μm are consistent with $n_e = 10^{3.5}$–10^4 cm^{-3}. The [Fe III] 2.348 μm/[Fe III] 2.218 μm ratio is 20% higher than its theoretical value, which is roughly constant over all of parameter space (Keenan et al. 1992), but [Fe III] 2.348 μm is blended with Pf29 and subject to measurement errors that are larger than the difference in extinctions in question (see Fig. 3). Even the minimum value that we infer for this ratio, with $A_K = 0$, is significantly greater than the model prediction. High values of [Fe III] 2.348 μm/[Fe III] 2.218 μm were also found by Luhman et al. (1998) in Orion. This discrepancy may be due to blending with another unknown line or to theoretical error; ratios from the latest calculations have an average deviation from the data of 10% (Keenan et al. 1992).

He I line ratios can be used to infer the nebular temperature T_e and are fairly insensitive to n_e. We find that the ratio of He I 2.1128 + 2.1137 μm to He I 2.0589 μm = 0.052 ± 0.003, which, for $n_e = 10^4$ cm^{-3}, is consistent with T_e = 17,500 ± 800 K (Benjamin, Skillman, & Smits 1999). However, this is much hotter than typical nebular temperatures and may indicate some nonnebular contribution from hot stars to the line emission.

The He I 2.0589 μm/Brγ ratio is an indicator of the $T_{\rm eff}$ of hot stars in H II regions (Doyon, Puxley, & Joseph 1992), although it is sensitive to nebular conditions such as the relative volumes and ionization fractions of He^+ and H^+, geometry, density, dustiness, etc. (Shields 1993). Doherty et al. (1995) studied H and He excitation in a sample of starburst galaxies and H II regions. For starbursts, they found evidence for high-$T_{\rm eff}$, low-n_e (~10^2 cm^{-2}) ionized gas from He I 2.0589 μm/Brγ ratios of 0.22–0.64. This is consistent with giant extended

TABLE 1

CLUSTER [Fe III] LINE RATIOS[a]

TRANSITION	REST λ[b] (μm)	OBSERVED RATIO	MODEL RATIO[c] 10^3	10^4	10^5
$^3G_3$–$^3H_4$	2.1457	0.14 ± 0.02	0.10	0.17	0.34
$^3G_5$–$^3H_6$	2.2183	1.00	1.00	1.00	1.00
$^3G_4$–$^3H_4$	2.2427	0.28 ± 0.02	0.26	0.29	0.38
$^3G_5$–$^3H_5$	2.3485	0.80 ± 0.03[d]	0.66	0.66	0.66

[a] The ratios are dereddened fluxes relative to [Fe III] 2.2183 μm, for which the dereddened flux was 9.11×10^{-16} ergs s^{-1} cm^{-2}.

[b] From Sugar & Corliss 1985.

[c] The models are for $T_e = 10^4$ K, with values of n_e in units of cm^{-3} (Keenan et al. 1992).

[d] The flux is determined by subtracting the Pf29 contribution that was obtained for the best-fit Landini extinction curve with A_K = 1.1 mag.

H II regions that are expected to dominate the emission-line spectra of typical starbursts. The ultracompact H II regions were characterized by higher ratios (0.8–0.9) and higher densities (~10^4 cm^{-3}). The cluster has a flux ratio of 0.70, which falls between the ratios of the two object classes of Doherty et al. (1995). Assuming the line emission is purely nebular, this ratio is consistent with a high-density (10^4 cm^{-3}) model of Shields (1993) and implies $T_{\rm eff} \simeq 39{,}000$ K for the assumed model parameters. This temperature is similar to that derived by Kunze et al. (1996), ≃44,000 K, from mid-IR *ISO* Short-Wavelength Spectrometer line observations in a large aperture on the overlap region of the Antennae.

The cluster has properties more like those of a compact H II region than a diffuse one. It appears to be a young, hot, high-density H II region, one of the first to form in this part of the Antennae interaction region (see Habing & Israel 1979 for a review of compact H II regions).

3.2. *Molecular Emission*

The spectrum shows evidence for almost pure UV fluorescence excited by FUV radiation from the O and B stars; the strong, vibrationally excited 1–0, 2–1, and 3–2 H_2 emission has $T_{\rm vib} \gtrsim 6000$ K and $T_{\rm rot} \simeq 970$, 1600, and 1800 K, respectively, and weak higher v (6–4, 8–6, and 9–7) transitions are present as well. The H_2 lines are extended over ≃200 pc, about twice the extent of the continuum and nebular line emission, so a significant fraction of the FUV (912–1108 Å) light escapes from the cluster to heat and photodissociate the local molecular ISM.

We obtained the photodissociation region (PDR) models of Draine & Bertoldi (1996) and compared them with our data by calculating reduced χ^2_ν. Models with high densities ($n_{\rm H} = 10^5$ cm^{-3}), moderately warm temperatures (T = 500–1500 K at the cloud surface), and high FUV fields ($G_0 = 10^3$–10^5 times the mean interstellar field) can reasonably fit the data. Figure 4 shows χ^2_ν contours for all models projected onto the $n_{\rm H}$-G_0 plane. The best-fit Draine & Bertoldi model is n2023b, which has $n_{\rm H} = 10^5$ cm^{-3}, T = 900 K, and G_0 = 5000. We fitted 22 H_2 lines, excluding 3–2 $S(2)$ 2.287 μm because it appears to be blended with a strong unidentified nebular line at 2.286 μm that is found in higher resolution spectra of planetary nebulae (Smith, Larson, & Fink 1981). The weak high-v transitions are all underpredicted by this model and appear to come from lower density gas ($n_{\rm H} \lesssim 10^3$–10^4 cm^{-3}) that is exposed to a weaker FUV field ($G_0 \lesssim 10^2$–10^3).

The ortho/para ratio of excited H_2, which we infer from the relative column densities in $v = 1$, $J = 3$ and $J = 2$, is the flux

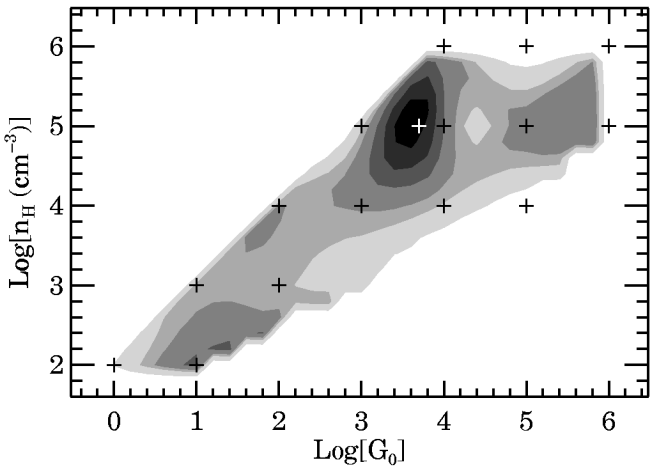

FIG. 4.—Comparison of H_2 line strengths with PDR models. The contours of χ^2_ν for 22 lines projected onto the n_H-G_0 plane peak at $n_H \sim 10^5$ cm^{-3} and $G_0 \sim 5000$. Model points (*plus signs*) are for T_0 = 300–2000 K. The white plus sign marks the best-fit PDR model of Draine & Bertoldi, with T_0 = 900 K and χ^2_ν = 9.3. The contours are 50, 25, 20, 15, 12, and 10.

ratio of the 1–0 $S(1)$ to $S(0)$ lines, 1.62 ± 0.07. This is consistent with the ground state $v = 0$, $J = 1$ and $J = 0$ H_2 being in LTE with an ortho/para ratio of 3 if the FUV absorption lines populating the non-LTE excited states are optically thick (Sternberg & Neufeld 1999). Indeed, the best-fit PDR models have temperatures that are comparable to T_{rot} in the lowest excited states as well as to the warm gas kinetic temperature in the Galactic PDR M16, T = 930 ± 50 K, measured by Levenson et al. (2000).

If the extent of the H_2 emission indicates that the mean free path of a FUV photon is ~200 pc, then $\langle n_H \rangle = 3$ cm^{-3} for a Galactic gas-to-dust ratio, while in the PDRs, $n_H = 10^4$–10^6 cm^{-3}. This implies that the molecular gas is extremely clumpy, which is consistent with the range of densities inferred from the detection of anomalously strong $v = 8$–6 H_2 emission.

4. NGC 4039 NUCLEUS

The spectrum of the nucleus of NGC 4039 is marked by a strong stellar continuum and bright, extended H_2 emission. Strong photospheric Mg I, Na I, and Ca I absorption and CO $\Delta v = 2$ bands indicate that the continuum is dominated by old giants. The CO band head is stronger than that of a M2 III star, suggesting some contribution from red supergiants. The absence of Brγ emission implies that star formation is currently extinct in the nucleus. Spatially extended, collisionally excited H_2 emission in the nucleus may be excited by S/N shocks from the last generation of nuclear star formation or by merger-induced cloud collisions. We defer detailed analysis of the nuclear spectrum to a later paper.

5. CONCLUSIONS

The highest surface brightness mid-IR peak in the *ISO* map of the Antennae galaxies is a massive (~16×10^6 $M_\odot$), obscured ($A_V \sim 9$–10), young (~4 Myr) star cluster with a half-light radius of ~ 32 pc, whose strong FUV flux excites the surrounding molecular ISM on scales of up to 200 pc. The cluster spectrum is dominated by extended fluorescently excited H_2 emission from clumpy PDRs and nebular emission from compact H II regions. In contrast, the nearby nucleus of NGC 4039 has a strong stellar spectrum dominated by cool stars, where the only emission lines are due to shock-excited H_2. These observations confirm the potential of near-infrared spectroscopy for exploration and discovery with the new generation of large ground-based telescopes. Our ongoing program of NIRSPEC observations promises to reveal a wealth of information on the nature of star formation in star clusters.

We acknowledge the hard work of past and present members of the UCLA NIRSPEC team: M. Angliongto, O. Bendiksen, G. Brims, L. Buchholz, J. Canfield, K. Chin, J. Hare, F. Lacayanga, S. Larson, T. Liu, N. Magnone, G. Skulason, M. Spencer, J. Weiss, and W. Wong. We thank Keck director F. Chaffee and all the CARA staff involved in the commissioning and integration of NIRSPEC, particularly instrument specialist T. Bida. We especially thank observing assistants J. Aycock, G. Puniwai, C. Sorenson, R. Quick, and W. Wack for their support. We also thank A. Sternberg for valuable discussions. We are grateful to R. Benjamin for providing us with He I emissivity data. A. M. G. acknowledges support from a NASA GSRP grant.

REFERENCES

Benjamin, R. A., Skillman, E. D., & Smits, D. P. 1999, ApJ, 514, 307
Doherty, R. M., Puxley, P. J., Lumsden, S. L., & Doyon, R. 1995, MNRAS, 277, 577
Doyon, R., Puxley, P. J., & Joseph, R. D. 1992, ApJ, 397, 117
Draine, B. T., & Bertoldi, F. 1996, ApJ, 468, 269
Fabbiano, G., Schweizer, F., & Mackie, G. 1997, ApJ, 478, 542
Habing, H. J., & Israel, F. P. 1979, ARA&A, 17, 345
Hummel, E., & van der Hulst, J. M. 1986, A&A, 155, 151
Hummer, D. G., & Storey, P. J. 1987, MNRAS, 224, 801
Hunter, D. A., Shaya, E. J., Holtzman, J. A., Light, R. M., O'Neil, E. J., Jr., & Lynds, R. 1995, ApJ, 448, 179
Keenan, F. P., Berrington, K. A., Burke, P. G., Zeippen, C. J., Le Dourneuf, M., & Clegg, R. E. S. 1992, ApJ, 384, 385
Kunze, D., et al. 1996, A&A, 315, L101
Landini, M., Natta, A., Salinari, P., Oliva, E., & Moorwood, A. F. M. 1984, A&A, 134, 284
Leitherer, C., et al. 1999, ApJS, 123, 3
Levenson, N. A., et al. 2000, ApJ, 533, L53
Luhman, K. L., Engelbracht, C. W., & Luhman, M. L. 1998, ApJ, 499, 799
McLean, I. S., etal. 1998, Proc. SPIE, 3354, 566
Mirabel, I. F., et al. 1998, A&A, 333, L1
Nikola, T., Genzel, R., Herrmann, F., Madden, S. C., Poglitsch, A., Geis, N., Townes, C. H., & Stacey, G. J. 1998, ApJ, 504, 749
Rieke, G. H., & Lebofsky, M. J. 1985, ApJ, 288, 618
Shields, J. C. 1993, ApJ, 419, 181
Smith, H. A., Larson, H. P., & Fink, U. 1981, ApJ, 244, 835
Stanford, S. A., Sargent, A. I., Sanders, D. B., & Scoville, N. Z. 1990, ApJ, 349, 492
Sternberg, A., & Neufeld, D. A. 1999, ApJ, 516, 371
Sugar, J., & Corliss, C. 1985, Atomic Energy Levels of the Iron-Period Elements, Potassium through Nickel (New York: American Chemical Society and AIP)
Whitmore, B. C., & Schweizer, F. 1995, AJ, 109, 960
Whitmore, B. C., Zhang, Q., Leitherer, C., Fall, S. M., Schweizer, F., & Miller, B. W. 1999, AJ, 118, 1551